JOURNAL OF GEOPHYSICAL RESEARCH, VOL. 115, D00K11, doi:10.1029/2009JD012812, 2010

Aerosol optical depth measurements in eastern China and a new calibration method

Kwon H. Lee,[1,2] Zhanqing Li,[1,3,4] M. C. Cribb,[1] Jianjun Liu,[3] Lei Wang,[3] Youfei Zheng,[3] Xiangao Xia,[4] Hongbin Chen,[4] and Bai Li[5]

Received 9 July 2009; revised 21 November 2009; accepted 10 December 2009; published 1 July 2010.

[1] We present a new calibration method to derive aerosol optical depth (AOD) from the MultiFilter Rotating Shadowband Radiometer (MFRSR) under extremely hazy atmospheric conditions during the East Asian Study of Tropospheric Aerosols: an International Regional Experiment (EAST-AIRE) and the Atmospheric Radiation Measurement (ARM) Mobile Facility (AMF) deployment in China. MFRSR measurements have been made at Xianghe since September 2004 and at Taihu and Shouxian since March and May 2008, respectively. Aerosol property retrievals from CIMEL Electonique, Paris, Sun and sky radiometers located at each site show that aerosol loading is substantial and highly variable during a given year (averaged daily $AOD_{550} = 0.80 \pm 0.14$). The conventional application of the Langley method to calibrate the MFRSR is not possible at these sites because there is a dearth of stable atmospheric and low-AOD conditions. To overcome this limitation of the traditional Langley plot method, highest irradiance values at a given air mass during a given period are used here. These highest values can represent the clear-sky and minimum aerosol loading conditions. A scatterplot of the AOD estimated by this method with the CIMEL Sun and sky radiometer AOD shows very good agreement: correlation coefficients are on the order of 0.98–0.99, slopes range from 0.93 to 0.97, and offsets are less than 0.02 for the three sites. AOD and Ångström exponents were derived from application of the method to all MFRSR data acquired at the three sites. AOD values at 500 nm are $\tau_{500} = 0.99 \pm 0.71$ ($\alpha_{500-870} = 1.45 \pm 0.59$) at Xianghe, 0.87 ± 0.54 (1.14 ± 0.31) at Taihu, and 0.84 ± 0.43 (1.15 ± 0.28) at Shouxian. Anthropogenic aerosols appear to dominate in the study region with significant contributions from large dust particles and influence of hydroscopic growth.

Citation: Lee, K. H., Z. Li, M. C. Cribb, J. Liu, L. Wang, Y. Zheng, X. Xia, H. Chen, and B. Li (2010), Aerosol optical depth measurements in eastern China and a new calibration method, *J. Geophys. Res.*, *115*, D00K11, doi:10.1029/2009JD012812.

1. Introduction

[2] Atmospheric aerosols influence the transfer of radiative energy by reflecting sunlight back to space [*Charlson et al.*, 1987], by absorbing solar radiation [*Hansen et al.*, 1997], and by interacting with clouds [*Twomey*, 1977]. In spite of these well-known mechanisms, aerosols still remain one of the major uncertainties in estimating the radiative forcing of climate change due to their nonuniform chemical and physical properties, and spatial and temporal variations in the atmosphere [*IPCC*, 2007]. Aerosol loading and properties must be accurately determined to improve our understanding of its direct and indirect effects.

[3] Aerosol optical depth (AOD) is a basic optical measurement of aerosol loading in the atmosphere. AODs have been measured from the ground using Sun and sky radiometers, most notably those of the Aerosol Robotic Network (AERONET) [*Holben et al.*, 1998]. AODs have also been retrieved from spaceborne satellite observations (for the latest review of algorithms and products, see *Lee et al.* [2009] and *Li et al.* [2009]). Satellites provide wide spatial coverage but poor temporal sampling; some inherent difficulties and uncertainties limit their retrieval accuracy [*Li et al.*, 2009]. Ground-based instruments measure the intensity of downwelling solar radiation reaching the detector from which AOD can be estimated at much higher temporal resolutions and with more accuracy.

[4] In addition to the widely used CIMEL Sun and sky radiometers that were designed with AOD studies in mind, the Multifilter Rotating Shadowband Radiometer (MFRSR)

[1] ESSIC, Department of Atmospheric and Oceanic Science, University of Maryland, College Park, Maryland, USA.
[2] Now at Department of Satellite Geoinformatics Engineering, Kyungil University, Gyeongsan, South Korea.
[3] College of Environmental Science and Engineering, Nanjing University of Information Science and Technology, Nanjing, China.
[4] LAGEO, Institute of Atmospheric Physics, Chinese Academy of Sciences, Beijing, China.
[5] Center for Atmospheric Observation, China Meteorological Administration, Beijing, China.

0148-0227/10/2009JD012812

Table 1. Location of MFRSR Measurement Stations and Data Availability[a]

Station	Latitude (deg)	Longitude (deg)	Elevation (m)	Available Data
Xianghe	39.754	116.962	36	September 2004 to June 2005, February 2006 to September 2007, and March 2008 to October 2008
Taihu	31.421	120.215	20	May 2008 to present
Shouxian (AMF)	32.558	116.782	22	May 2008 to December 2008

[a]MFRSR, MultiFilter Rotating Shadowband Radiometer; AMF, Atmospheric Radiation Measurement (ARM) Mobile Facility.

is another instrument that can be used to determine aerosol optical properties, as well as cloud optical properties [*Harrison et al.*, 1994]. The MFRSR measures total and diffuse solar irradiances at six narrowband wavelength channels centered at 0.415, 0.500, 0.615, 0.673, 0.870 and 0.940 μm. Direct solar irradiances obtained by subtracting diffuse radiation from total irradiances are used to derive spectral AODs after calibration of the sensor. Langley regression is a method widely used to analyze direct-beam extinction measurements under different atmospheric opacity conditions that arise from changes in aerosol loading and atmospheric constituents [*Shaw et al.*, 1973; *Shaw*, 1976; *Harrison and Michalsky*, 1994; *Michalsky et al.*, 2001; *Augustine et al.*, 2003]. Another method used by *Tanaka et al.* [1986] involved the retrieval of AODs from the calibration of diffuse radiation measurements. *Alexandrov et al.* [2002] used direct-to-diffuse ratios to correct the direct-beam optical depth. The diffuse and direct irradiances measured by the MFRSR are also used to estimate other aerosol optical and microphysical properties, such as the single scattering albedo (SSA), the asymmetry parameter, and the aerosol size distribution [*Petters et al.*, 2003; *Kassianov et al.*, 2005, 2007; *Alexandrov et al.*, 2008; *Ge et al.*, 2010].

[5] Extensive aerosol observations, as well as measurements of other meteorological variables, have been made in China under the auspices of the East Asian Study of Tropospheric Aerosols: an International Regional Experiment (EAST-AIRE) [*Li et al.*, 2007a] and the Atmospheric Radiation Measurement (ARM) Mobile Facility (AMF) deployment in China [*Li et al.*, 2008]. The first EAST-AIRE site was established in late 2004 at Xianghe and MFRSR measurements have been made since then. Two additional MFRSR instruments were installed at Shouxian and Taihu in March 2008 as part of the deployment of the ARM AMF. A summary of the geographic locations of these sites and data availability is given in Table 1. As shown in Figure 1, all three stations are located in the most developed regions of China and ambient aerosol loadings are typically very high [*Li et al.*, 2007b]. Dramatic day-to-day variations in aerosol loading and variable absorbing characteristics of regional aerosols were also found over the eastern part of China during the EAST-AIRE [*Xia et al.*, 2007; *Mi et al.*, 2007; *Lee et al.*, 2007]. These variations may incur large uncertainties in remotely sensed AODs. To decrease this uncertainty in aerosol retrievals from the MFRSR, we propose a new calibration method that can extend the capability of MFRSRs operating under highly variable atmospheric conditions for which the conventional Langley method has been deemed invalid or impractical. This paper is organized as follows. Section 2 describes the general nature of the Langley calibration method. In section 3, we present our approach and compare the results with those from AERONET retrievals. The variations in AOD retrievals are discussed in section 4. Finally, the study is summarized in section 5.

2. Calibration Uncertainties Using Langley Plots

[6] Calibration of solar radiation measurements by any instrument is a key step in obtaining AOD retrievals [*Reagan et al.*, 1986; *Schotland and Lea*, 1986; *Harrison and Michalsky*, 1994]. Due to the unstable spectral response of any Sun and sky radiometers, periodic calibration is necessary. Langley regression has generally been used to retrieve AODs from MFRSR-measured irradiances. Top-of-the atmosphere (TOA) solar irradiance (I_o) is first estimated using a Langley plot, which is based on the Beer-Lambert equation. The instantaneous direct solar irradiance (I) measured by the MFRSR can be represented as

$$I = I_0 \exp(-\tau m). \tag{1}$$

Taking the logarithm of both sides, equation (1) becomes

$$\ln I = \ln I_0 - \tau m, \tag{2}$$

where I_0 is the extraterrestrial solar irradiance, m is the air mass calculated as a function of the solar zenith angle, and τ is

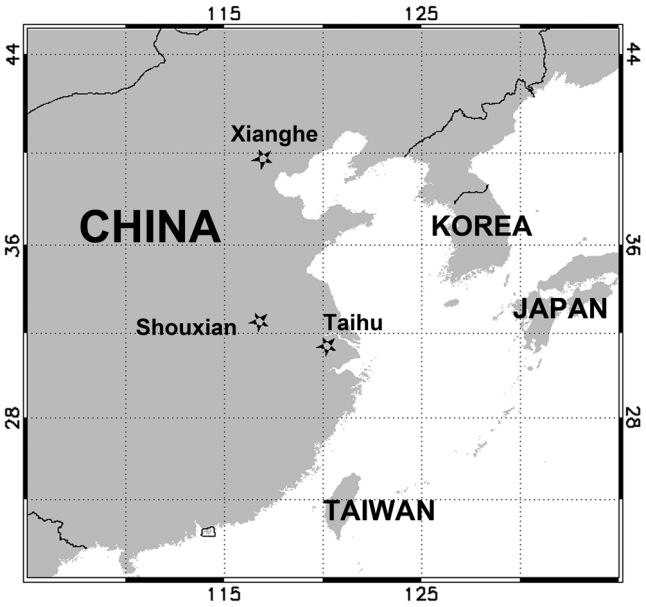

Figure 1. Geographic map of MultiFilter Rotating Shadowband Radiometer (MFRSR) measurement stations. Note that the Atmospheric Radiation Measurement (ARM) Mobile Facility (AMF) is located at Shouxian.

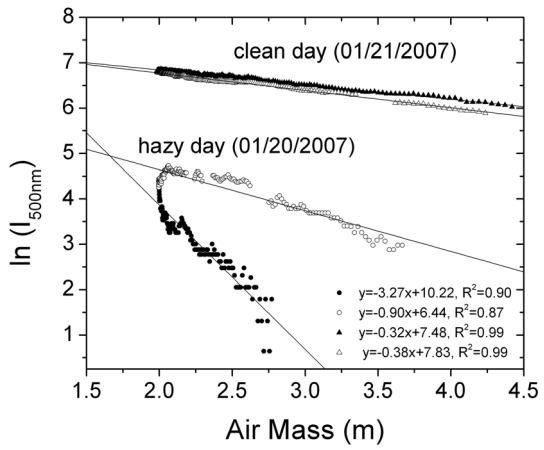

Figure 2. Langley plots for MFRSR 500 nm channel data obtained on 20 and 21 January 2007 in Xianghe, China. Solid and open symbols represent MFRSR-measured irradiances during the morning and afternoon, respectively.

the total optical depth (TOD) due to atmospheric attenuation. Using this linear equation, one can derive ln I_0 by measuring the ln I at different air masses (m) during the day. Stable atmospheric conditions are required during this period of time to obtain a unique I_0 [*Harrison and Michalsky*, 1994]. Aerosol loading in the atmosphere is generally variable so calibrations using the Langley method are usually restricted to regions with pristine atmospheric conditions or at least to regions where stable and low AODs frequently occur. The ideal location for applying the Langley method is in high-altitude remote mountainous regions such as Mauna Loa in Hawaii. Unfortunately, it is usually logistically difficult and economically too expensive to conduct calibrations at such sites. Performing calibrations under less ideal atmospheric conditions can lead to incorrect estimations of I_0 and errors in AOD retrievals.

[7] An illustration of this problem is shown in Figure 2 using MFRSR data obtained at Xianghe on 20–21 January 2007. In Figure 2, two different aerosol loading conditions are compared: hazy conditions on 20 January and pristine conditions on 21 January. From the AERONET data record, daily mean AOD values at 500 nm are 1.38 ± 0.30 on 20 January and 0.15 ± 0.03 on 21 January. A maximum AOD value of 1.77 occurred in the early morning of 20 January then dropped off sharply by noon and gradually decreased to 1.0 in the late afternoon. These variations in aerosol load lead to large differences in the y intercept of regression lines which in this example vary from 10.22 in the morning to 6.44 in the afternoon. Such a variation in aerosol loading during a given day would lead to two different Langley regression lines, each of which having a high correlation ($R^2 = 0.99$). The Langley method is therefore not valid for calibration purposes when AODs are highly variable.

[8] Errors in AOD are incurred from the use of an incorrect value of ln I_0. Using I_0' and τ' obtained from the incorrect Langley plot, equation (1) becomes

$$I = I_0' \exp(-\tau' m). \tag{3}$$

From equations (1) and (3), the error in AOD retrievals ($\Delta\tau = \tau' - \tau$) can be expressed as

$$\Delta\tau = \frac{1}{m}\ln\left(\frac{I_0'}{I_0}\right). \tag{4}$$

The relative error in I_0 is defined as $\varepsilon_{I_0} = \frac{I_0' - I_0}{I_0}$., equation (4) can then be rewritten as a function of ε_{I_0} and m in the following manner:

$$\Delta\tau = \frac{1}{m}\ln(\varepsilon_{I_0} + 1). \tag{5}$$

Figure 3 shows $\Delta\tau$ calculated using equation (5) with different ε_{I_0}(0–100%) and m (0–10.0) values. In general, $\Delta\tau$ is very sensitive to ε_{I_0} as m decreases. The maximum absolute error, $\Delta\tau_{\max}$, is 3.47 and occurs near noontime when m is close to 1. However, $\Delta\tau$ is not as sensitive to ε_{I_0} for larger m. This implies that the accuracy of the retrieved AOT significantly decreases toward noontime even for relatively small error in the Langley calibration. Because the Langley regression requires drastic changes in air mass, the air mass ranging from 2 to 5 is traditionally used to prevent slow changes near noon. The Langley techniques currently used for MFRSR include filtering and averaging of the time series of instantaneous I_0 [cf. *Michalsky et al.*, 2001]. More detailed description of the Langley analysis can be also found in the work of *Schmid et al.* [1998].

3. A New Solar Calibration Method

[9] The traditional Langley calibration approach is applied to a single day suitable for linear regression. I_0 values from these days are then filtered and averaged to obtain the calibration coefficients. However, this needs clean and homogeneous atmospheric condition during an individual day. The modified Langley method proposed here involves the acquisition of the maximum value composite (MVC) of the largest irradiance values at a given air mass during a period of time that is long enough and during which low-AOD conditions occur. Instead of a single day, data from multiple clear-sky days are employed. Due to statistical uncertainties, not all maximum values are valid. Anomalous values, such as zero or abnormally large/small values, must first be removed by screening out local minima. This is done by comparing values in neighboring air mass bins from which a standard deviation (SD) of relative difference is computed. A threshold of SD < 1% is required in each bin. Also, the MVC cannot deal with temporal changes in I_o during a given composite period, therefore, smoothing and removal of outliers by filtering technique [*Forgan*, 1988] were employed from one composite period to another.

[10] The I_o values determined by the proposed method highly depend on the period of time chosen. If the period of time is too long, information about the temporal variability is lost and if it is too short, there may be a dearth of valid data. There is no physical basis upon which to define the ideal time period so four different periods (5, 7, 10, and 30 days) were selected to test the sensitivity of the proposed method. AODs were calculated from these four different Langley calibrations (τ_{period}) and matched with AODs from AERONET ($\tau_{aeronet}$). CIMEL Sun and sky radiometers used in AERONET are

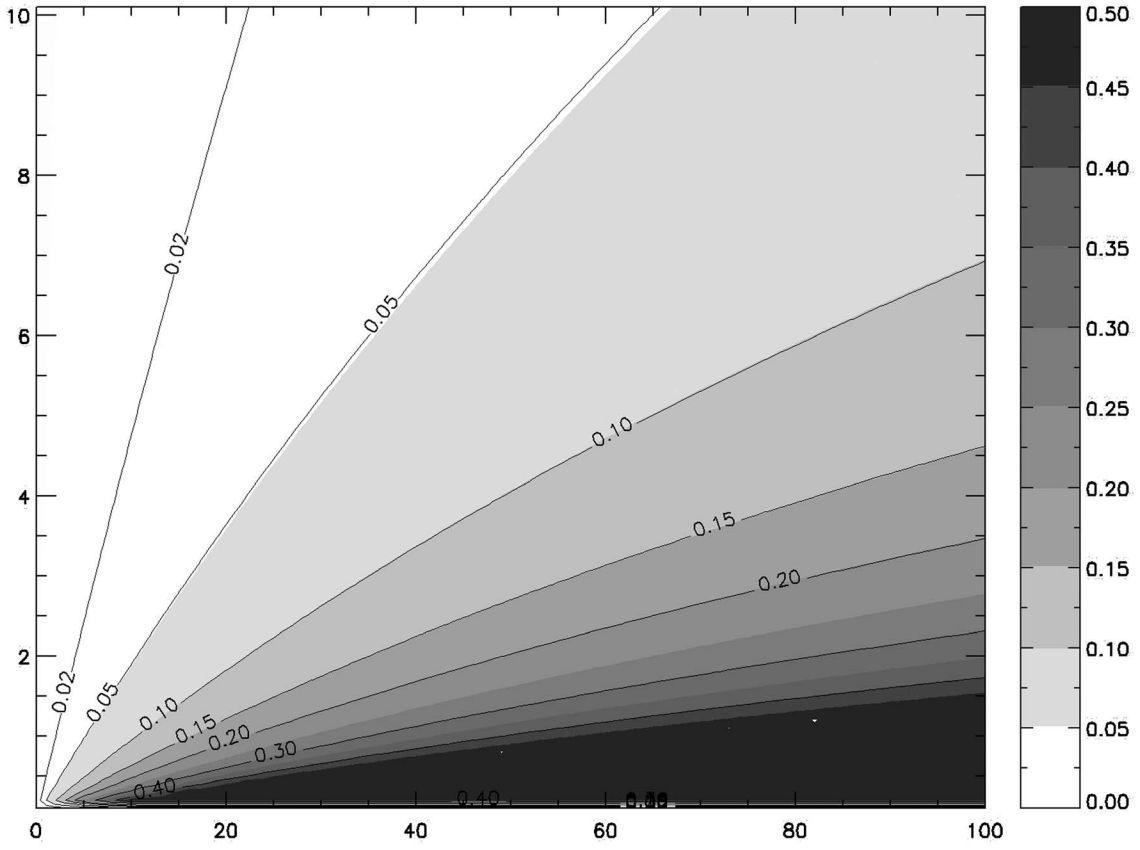

Figure 3. Aerosol optical depth (AOD) retrieval error ($\Delta\tau$) as a function of ε_{I_0} (%) and air mass (m).

calibrated by side-by-side comparisons to standard CIMELs that are Langley calibrated at Mauna Loa and then assumed stable until the end calibration of their deployment can verify their stability during their deployment. Errors in AOD ($\Delta\tau_e = \sqrt{\left(\tau_{period} - \tau_{aeronet}\right)^2}/\tau_{aeronet}$) were obtained by using randomly selected data from all measurements. $\Delta\tau_e$ for time periods of 5, 7, and 10 days are about 20% and equal to 7.5% for the period of 30 days. The 30 day period is used as a compromise between temporal changes in sensor sensitivity and acquiring enough data to perform a reliable MVC.

[11] Figure 4 shows an example of MVC values during April 2007 at the Xianghe site. The maximum direct irradiances at 81 air masses (from $m = 1$ to 5, bin size $\Delta m = 0.05$) were used to composite a single Langley plot. The number on regression line represents the day selected by MVC. Data from nine different days are used in this case. In Figure 4 (bottom), histogram shows the number of days used in a monthly MVC. These number ranges from 2 to 7. The regression line by MVC result is also compared with the best fitted Langley plots during the same period. Differences between I_0 by MVC regression and by single day Langley plots range from 9 to 38%. Those differences can lead to large error (0.01~0.4) in AOD determination.

[12] Figure 5 shows I_o values calculated at the three MFRSR measurement sites. Relatively small standard deviations in I_o during the whole period are found for Taihu (8.6%) and Shouxian (5.6%). At Xianghe, I_o values drift considerably

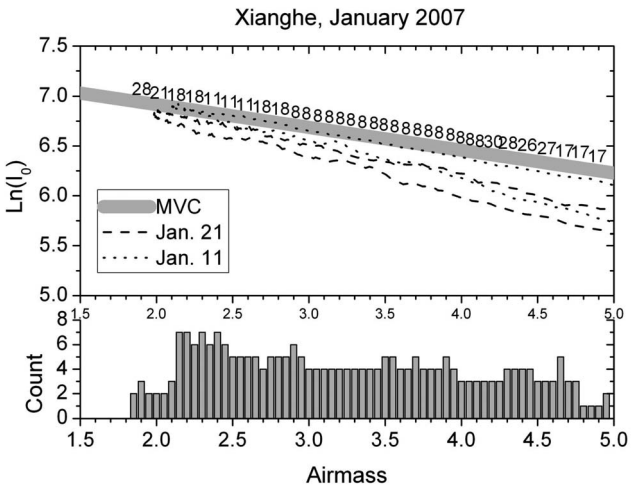

Figure 4. The maximum value composite (MVC) result at 500 nm for January 2007 and traditional Langley plots for 11 January (dotted line) and 21 January (dashed line). All linear correlation coefficients are larger than 0.99, and y intercepts for each plot are 7.372 (MVC), 7.457 (11 January, morning), 7.697 (11 January, afternoon), 7.504 (21 January, morning), and 7.546 (21 January, afternoon), respectively. Histogram represents number of days contributing to the MVC.

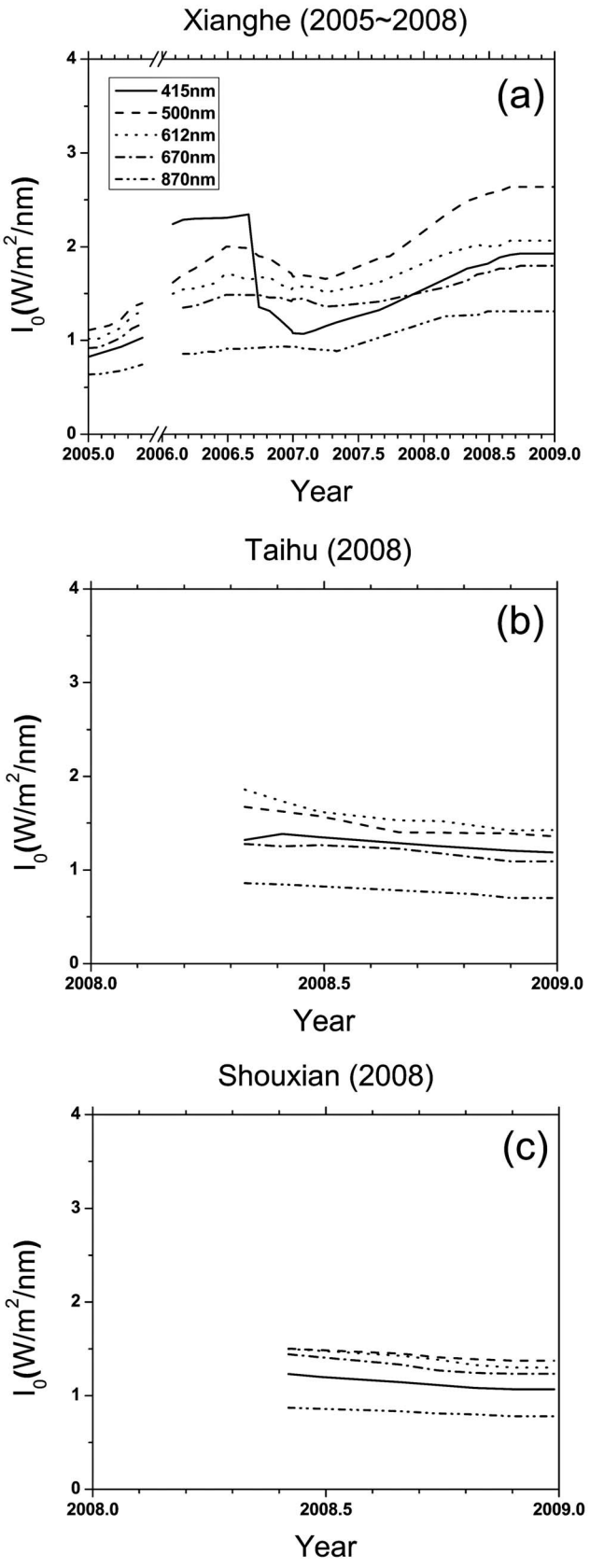

Figure 5. I_0 values derived in this study.

and the standard deviation is higher (~23%). This drift is particularly evident for the 415 nm channel during 2006. This large standard deviation poses a serious challenge for using the data to derive AODs.

[13] Using I_o values derived over 30 day time periods, TODs at 500 nm are calculated following equation (1). This equation is also used to derive TODs at the four other MFRSR channels at a 15 s temporal resolution. AODs are obtained from TODs by subtracting the contributions to extinction from Rayleigh scattering and gaseous absorption. Rayleigh scattering attenuates solar radiation reaching the ground in all six MFRSR channels while the major gaseous absorbers in these bands are O_3 (at 500, 615, and 670 nm) and NO_2 (at 415, 500, and 615 nm) [*Alexandrov et al.* 2002]. The Rayleigh optical depth (ROD) is parameterized as a function of wavelength and pressure [*Hansen and Travis*, 1974]:

$$\tau_{Ray} = 0.008569\lambda^{-4}\left(1 + 0.0113\lambda^{-2} + 0.00013\lambda^{-4}\right) \quad (6)$$

where λ is the wavelength in μm. Total column ozone amount data from the Total Ozone Mapping Spectrometer (TOMS) or Ozone Monitoring Instrument (OMI) satellite are used to calculate the ozone optical depth (OOD). OOD is a product of total column ozone (D_{O3}) in Dobson units (1 DU = 10^{-3} atm-cm = 2.687 × 10^{16} molecules cm^{-2}) and ozone absorption coefficients (σ_{O3} in cm^{-1}) from *Nicolet* [1981]:

$$\tau_{O3} = \sigma_{O3} \times D_{O3}/1000. \quad (7)$$

The TOMS instrument measures total column ozone data at a horizontal resolution of 1–1.25° and with a 2% RMS error (TOMS Ozone Algorithm Theoretical Basis Document, available at http://toms.gsfc.nasa.gov/version8/v8toms_atbd.pdf). Over the study area, the annual mean ozone amount is 300 ± 40 DU. The error in OOD due to this ozone retrieval error is about 0.0007 at 615 nm where ozone absorption is at its maximum.

[14] In a similar manner, total column NO_2 (D_{NO2}) measured from the OMI satellite and averaged NO_2 values during 2005~2008 for Xianghe, Taihu, and Shouxian are 0.519 ± 0.201, 0.416 ± 0.229, and 0.362 ± 0.199 DU, respectively. NO_2 absorption cross sections (σ_{NO2}) from *Vandaele et al.* [2002] were used to calculate the NO_2 optical depth (NOD):

$$\tau_{NO2} = \sigma_{NO2} \times D_{NO2}/1000. \quad (8)$$

A recent validation study over eastern China reported that the OMI NO_2 data (version 3) has a positive bias of 1.6 × 10^{15} molecules cm^{-2} [*Irie et al.*, 2008]. Sensitivity analyses using this bias show that the absolute error in NOD is 0.0008 at 415 nm, a very small contribution to AOD retrievals.

[15] Simultaneous estimates of AOD from MFRSRs located at the three measurement sites and from collocated CIMEL Sun and sky radiometers (data available from http://aeronet.gsfc.nasa.gov/) are compared. Same CIMEL instruments for three sites are operated. It has 8 channels and their wavelengths are 340,380, 440, 500, 675, 870, 1020, and 1640 nm. Figure 6 shows MFRSR AOD in comparison with CIMEL AOD at four wavelengths. The least square fit is drawn with a

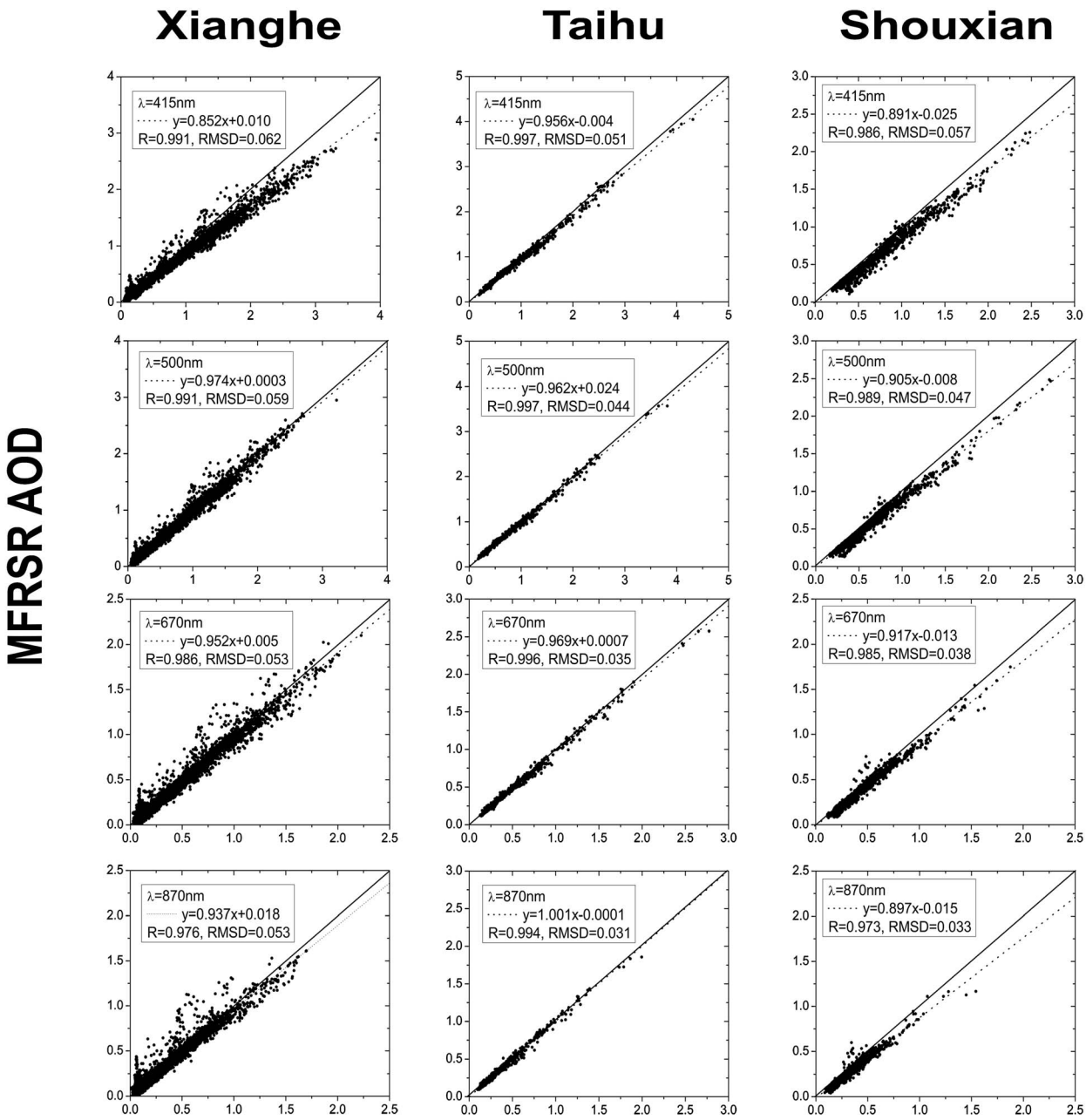

Figure 6. MFRSR AOD as a function of CIMEL AOD at (top to bottom, respectively) 415, 500, 670, and 870 nm.

dashed line and the solid line is the 1:1 line for comparison purposes. The slopes of the linear fits are close to 1.0 and offsets are less than 0.02. The MFRSR results are generally consistent with the CIMEL results with discrepancies on the order of 1% to 10%. In general, results from the suggested MVC calibration agree with those of the AERONET method to within the error of this approach. It is worthy to note that residual optical depth may influence systematic error even for a large set of Langley plots [*Shaw*, 1976]. Actually it depends on the diurnal cycle of aerosol sources and local meteorology for each measurement site. If this is the case, we have a part of systematic error which cannot be deduced or quantified from the collected data set alone. However, in view of the highly variable nature of the measurements and uncertainties in the new calibration method, the agreement is encouraging. This suggests that even under the heavy and highly variable aerosol loading conditions prevalent at these sites, our method can be used to calibrate the MFRSR.

[16] Larger errors, however, on the order of about 6% to 15%, are found at the 415 nm channel, which is presumably caused, at least partially, by extrapolation of the CIMEL AOD data. Because the CIMEL Sun and sky radiometer does not have a 415 nm channel, the 500 nm AODs were extrapolated to 415 nm using the Ångström exponent. Blocking of

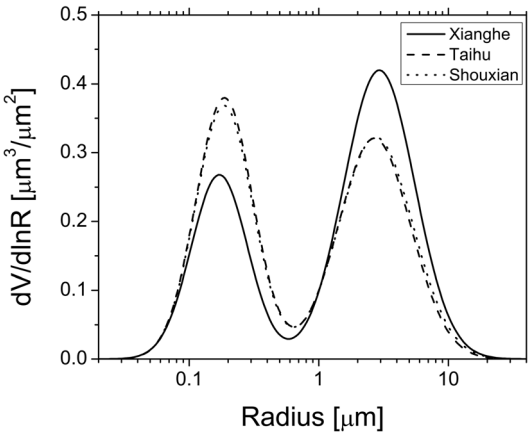

Figure 7. Particle size distributions derived by Aerosol Robotic Network (AERONET) inversion algorithm [*Dubovik and King*, 2000].

some forward scattered solar radiation is likely the cause for the small but systematic biases shown in Figure 6. Diffuse radiation (I_{dif}) is calculated using the following relationship:

$$I_{dif} = I_{blk} + [I_{tot} - (I_{side1} + I_{side2})/2], \quad (9)$$

where I_{blk} is the radiation measurement made in the shade under the shadowband (umbral angle of ~3.27°), I_{tot} is the global irradiance measured without the shadowband, and $I_{side1,2}$ are two sideband measurements taken to estimate the solar aureole contribution which is missing because the shadowband shades a portion of the sky.

[17] Mean particle size distributions at three sites are shown in Figure 7. At Xianghe, the averaged fine mode volume fraction is found to be 33.7% but the other sites are 48.4% (Taihu) and 46.9% (Shouxian). The fine mode volume fraction (33.7%) at Xianghe is lower than those found in the other sites (48.4 at Taihu and 46.9% at Shouxian). These values are close to those urban-industrial types found in the work of *Dubovik et al.* [2002]. Those particles have large scattering cross section at shorter wavelength. Based on this information, calculated phase functions show higher forward scattering ratio of 0.8 at 415 nm and lowest 0.6 at 870 nm, confirming that a significant fraction of the forward scattering is obscured by the MFRSR strip band. Given MFRSR umbral angle of 3.27, the band blocks a strip of sky. To estimate the portion of diffuse irradiance that is blocked by the band, irradiances blocked by sphere (Blk_{Sph}) and strip (Blk_{Str}) were simulated at each MFRSR bands. It can be considered that Blk_{Sph} and Blk_{Str} are true, and MFRSR measured diffuse irradiance. The simulations show that the Blk_{Sph} and Blk_{Str} are higher at the shorter wavelength (Table 2). Also, their differences are slightly higher at the shorter wavelength; that can underestimate diffuse and overestimate direct. The overall effect is underestimation of AOD.

4. Aerosol Optical Properties During EAST-AIRE and the AMF Deployment

[18] Note that while CIMEL Sun and sky radiometers were installed at all three sites, data gaps exist due to various reasons (e.g., removal for calibration, instrument failure, etc.) The presence of two independent instruments at a site helps provide (1) more complete and continuous data and (2) cross-checking as a means of data quality control. Time series of the daily mean AODs at 500 nm for Xianghe, Taihu, and Shouxian during the EAST-AIRE and AMF deployment period are shown in Figure 8. The magnitude and variability of daily AOD values often exceed 1 throughout the year, which is likely due to variability in the emissions of local sources and meteorology. AODs tend to be large from late spring to summer. Daily mean AODs range from as low as 0.05 during winter to over 2.0 during summer. This is probably a result of the Asian dust storms active during the spring, increased human activity (e.g., biomass burning in agricultural fields and pollution in urban areas) and the hygroscopic growth of particles in the hot wet summer season.

[19] Time series of Ångström exponents in 2008, which are derived from AODs at 500 and 860 nm, are shown in Figure 9. In general, the lowest seasonal mean values are found during winter (1.01) for Shouxian and spring season (0.98) at Xinghe, while largest values (1.42) at Xiaghe are observed during the summer. In spring, these low Ångström exponents together with high AODs indicate Asian dust storm events which is reinforced by the negative correlations between AOD and Ångström exponent at Xianghe (see Figure 10). Positive correlations between AOD and Ångström exponent at the other sites is seen, which implies the presence of more fine-mode pollution or smoke aerosols.

[20] Table 3 provides statistics for AODs and Ångström exponents at the three sites. At Xianghe, about 70 km east of Beijing, the annual mean daily AOD and Ångström exponent during 2005–2008 are $\tau = 0.77 \pm 0.60$ and $\alpha = 1.11 \pm 0.49$, respectively; higher values are observed during 2008 ($\tau = 0.99 \pm 0.71$ and $\alpha = 1.54 \pm 0.65$). The mean AOD and Ångström exponent at the two more southern sites during 2008 are about $\tau = 0.85 \pm 0.49$ and $\alpha = 1.15 \pm 0.29$. The standard deviations in AODs at all sites are greater than 50% of the mean AODs, indicating that AODs are highly variable throughout the year. Although AODs at all stations are high with strong day-to-day variations, differences in annual mean AOD and Ångström exponent values between northern and southern stations suggest that the aerosol types and burdens are different. These findings with regard to geographic dif-

Table 2. Forward Scattering by Aerosol Microphysics From Figure 7 and Simulated Irradiance Blocked by Sphere and Strip[a]

Station	Parameter	MFRSR Band Wavelength				
		415 nm	500 nm	612 nm	670 nm	860 nm
Xianghe	R_F	0.760	0.701	0.644	0.624	0.579
Xianghe	Blk_{Sph}	0.247	0.228	0.209	0.203	0.188
Xianghe	Blk_{Str}	4.333	3.996	3.671	3.555	3.301
Xianghe	ΔBlk	−4.086	−3.768	−3.462	−3.353	−3.113
Taihu	R_F	0.806	0.744	0.681	0.657	0.604
Taihu	Blk_{Sph}	0.262	0.242	0.221	0.213	0.196
Taihu	Blk_{Str}	4.598	4.242	3.881	3.744	3.444
Taihu	ΔBlk	−4.336	−4.000	−3.660	−3.531	−3.247
Shouxian	R_F	0.782	0.718	0.657	0.634	0.585
Shouxian	Blk_{Sph}	0.254	0.233	0.214	0.206	0.190
Shouxian	Blk_{Str}	4.460	4.095	3.746	3.617	3.335
Shouxian	ΔBlk	−4.206	−3.861	−3.533	−3.411	−3.145

[a] R_F, forward scattering ratio (forward scattering/total scattering); Blk_{Sph}, % of blocked irradiance by sphere; Blk_{Str}, % of blocked irradiance by strip; ΔBlk, $Blk_{Str} - Blk_{Sph}$.

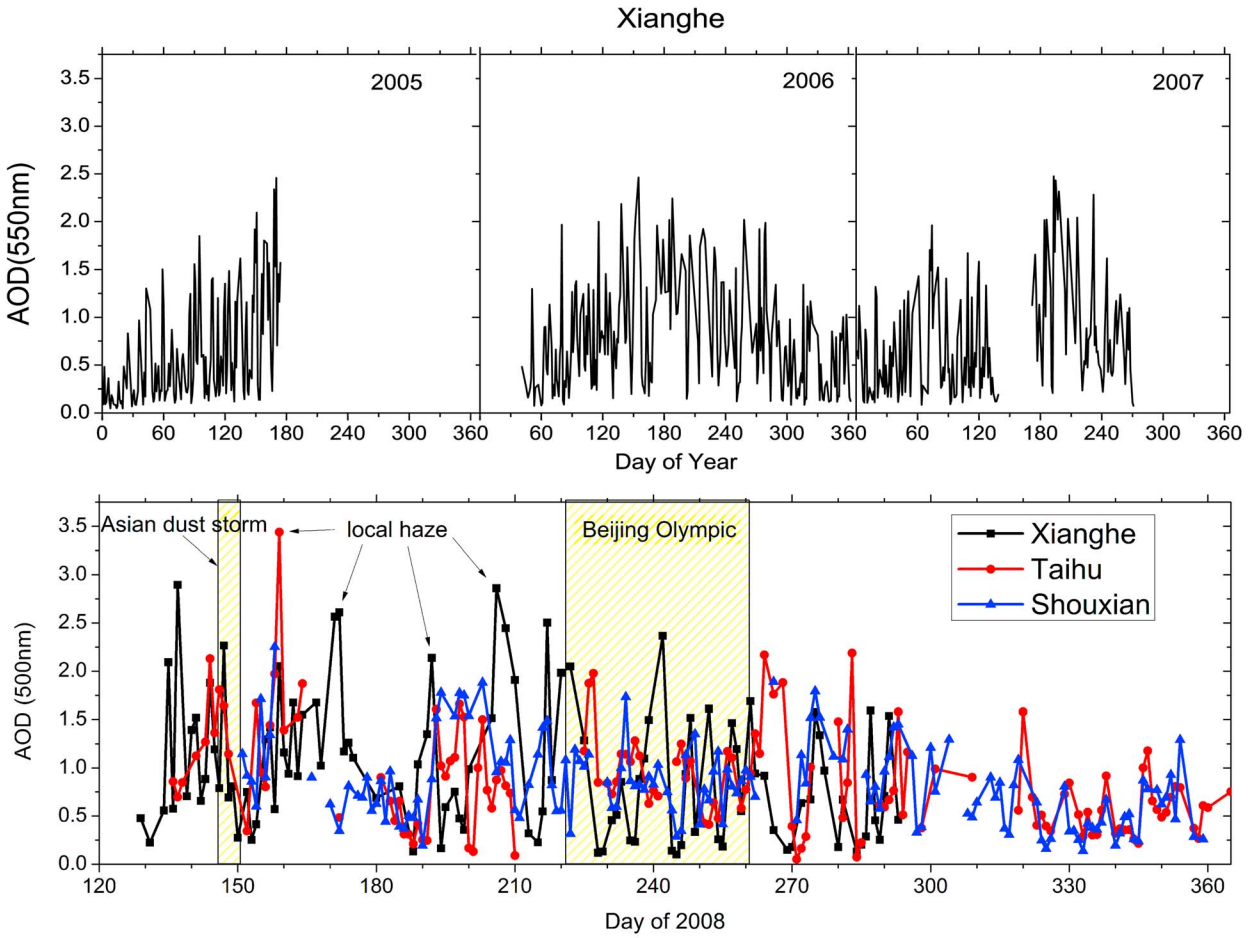

Figure 8. Time series of MFRSR daily mean AOD at 500 nm.

ferences are similar to patterns seen in satellite-retrieved AOD and fire pixel counts maps (Figure 11). In Figure 11, Terra/MODIS Level 3 aerosol products (Collection 5) are shown. The numerous fire pixel counts near Taihu indicates that biomass burning aerosols are commonly present in the area. The aerosol burden at Xianghe may originate from urban pollution, as well as from dust storms during the spring season.

[21] AOD data can be used to study major episodes of heavy aerosol loading such as from dust storms and from local/transported haze/smoke at each station. Figure 12 presents satellite images which clearly show dust and haze

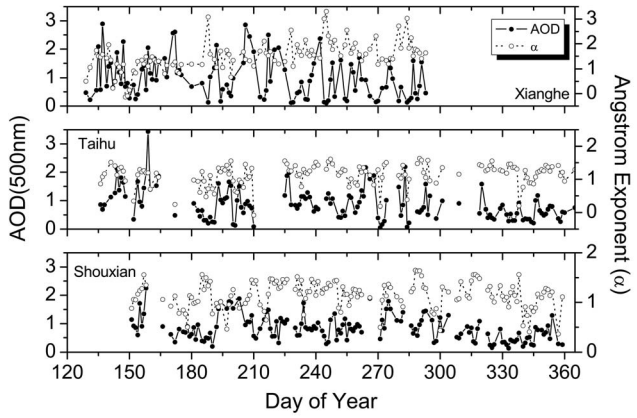

Figure 9. Time series of daily mean AOD at 500 nm and Ångström exponents for (top to bottom, respectively) Xianghe, Taihu, and Shouxian.

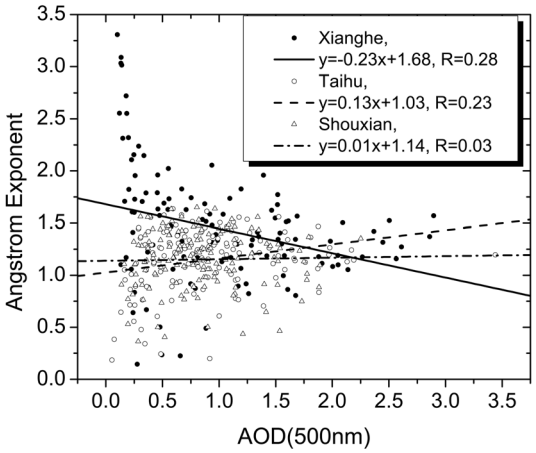

Figure 10. Ångström exponent as a function of AOD for the three sites in 2008.

Table 3. MFRSR AOD and Ångström Exponent Statistics for Each Station[a]

		AOD (λ = 500 nm)			Ångström Exponent (λ = 500–870 nm)		
Station	Year	Max	Min	Mean	Max	Min	Mean
Xianghe	2005	2.46	0.05	0.61 ± 0.56	2.11	0.18	1.14 ± 0.39
Xianghe	2006	2.46	0.08	0.77 ± 0.55	1.66	0.09	0.96 ± 0.38
Xianghe	2007	2.47	0.08	0.72 ± 0.55	1.81	0.03	1.00 ± 0.41
Xianghe	2008	2.9	0.1	0.99 ± 0.71	3.39	0.16	1.54 ± 0.65
Taihu	2008	3.44	0.05	0.87 ± 0.54	1.61	0.20	1.14 ± 0.30
Shouxian	2008	2.25	0.14	0.84 ± 0.43	1.62	0.09	1.15 ± 0.28

[a]AOD, aerosol optical depth.

plumes for such case studies. As a demonstration, results from a dust episode observed from Xianghe to Taihu on 27–30 May 2008 were examined. Relatively high AODs (~1.1) and low Ångström exponents (~0.1) attest to the existence of large dust particles. On 5 June 2008, a strong haze case was observed at Taihu when AODs peaked at ~3.4 and the Ångström exponent was ~1.2.

[22] Other notable hazy days are 24–26 July 2008 at Xianghe. After 20 July 2008, prior to the Beijing Olympic games (8 August to 17 September 2008), the Chinese government placed strict controls on local emissions. During the Olympic Games, the AODs were less than usual but still had large fluctuations. These fluctuations were primarily the result of weather conditions and the geographical characteristic of this region which may allow air pollutants to accumulate.

5. Conclusions

[23] MFRSR measurements collected during the EAST-AIRE and the AMF deployment in Xianghe, Taihu, and Shouxian, China are used here to derive AOD. The generally heavy aerosol loading and strong variations in AOD at these stations make it nearly impossible to find days that meet the requirements for performing Langley analyses. To overcome this limitation, we propose a new method which uses the largest irradiance values measured at a given air mass interval over a certain period of time. One month was selected as the period of time to use to derive AODs with this data.

[24] AODs estimated from MFRSR data at all three stations using our new method agree very well with those from CIMEL Sun and sky radiometer retrievals. The slope of the linear fit between the two sets of AOD is close to 1.0 and

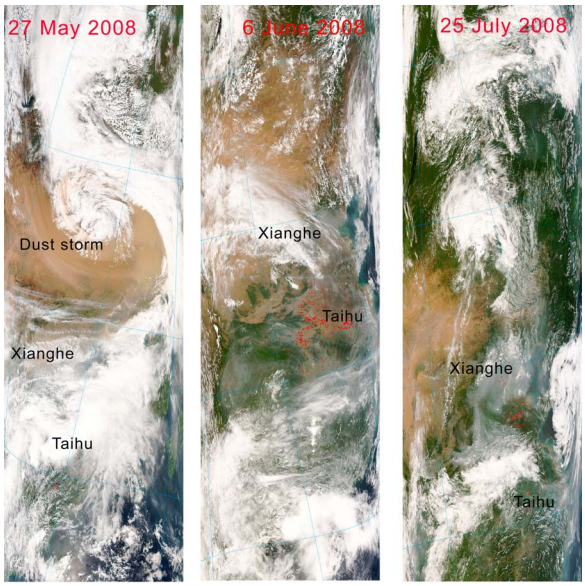

Figure 12. MODIS RGB color composite images for (left) the dust case on 27 May 2008 and the smoky haze cases on (middle) 6 June 2008 and (right) 25 July 2008. The red dots show the location of hot spots.

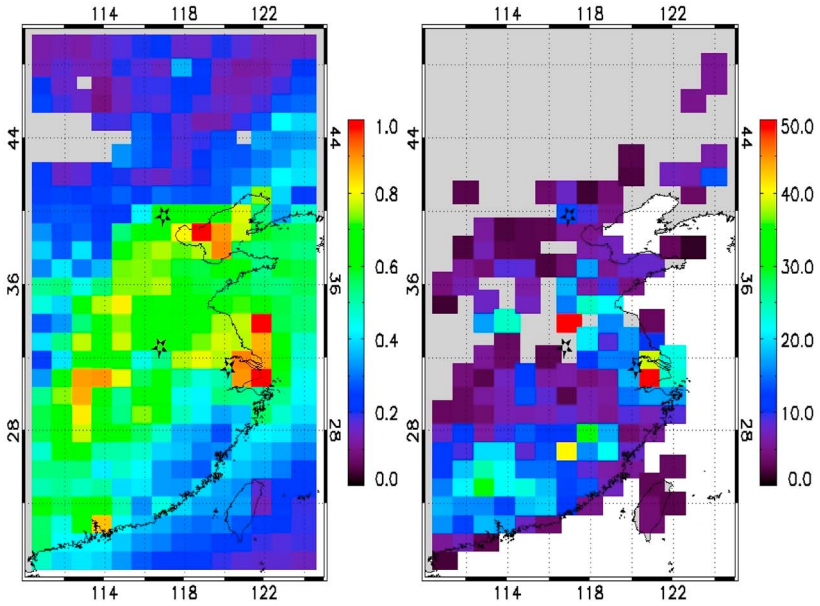

Figure 11. Annual mean (left) MODIS-retrieved AOD and (right) fire pixel counts. Star symbols show the locations of the three sites.

offsets are smaller than 0.02; the RMSD is smaller than 6%. These results suggest that the proposed method is valid and useful for solar calibration of MFRSRs under heavy and variable aerosol load conditions.

[25] Statistical analysis of the daily averaged AODs at 500 nm reveals that AODs in the summertime are generally higher than in winter. There are several days during the measurement campaign when the AODS were large (>1.5). The Ångström exponent exhibits seasonal variability and is largest during the summer and smallest during the Asian dust storm season. The MFRSR-retrieved AOD and Ångström exponent differed significantly between dust and haze cases. This can lead to differences in their direct radiative effects on subregional scales.

[26] **Acknowledgments.** OMI NRT data were provided by KNMI (Netherlands) and were produced in collaboration with NASA (United States). OMI, a Dutch-Finnish built instrument, is part of NASA's EOS-Aura payload. The OMI project is managed by NIVR and KNMI in the Netherlands. The study was funded by the NASA Radiation Science program (NNX08AH71G), DOE's Atmospheric Radiation Measurement (ARM) program (DEFG0208ER64571), and MOST's 973 National Basic Research program (2008CB403706). Xiangao Xia is supported by the National Science Foundation of China (40775009).

References

Alexandrov, M. D., A. A. Lacis, B. E. Carlson, and B. Cairns (2002), Remote sensing of atmospheric aerosols and trace gases by means of multifilter rotating shadowband radiometer. Part I: Retrieval algorithms, *J. Atmos. Sci.*, *59*, 524–543, doi:10.1175/1520-0469(2002)059<0524:RSOAAA>2.0.CO;2.

Alexandrov, M. D., A. A. Lacis, B. E. Carlson, and B. Cairns (2008), Characterization of atmospheric aerosols using MFRSR measurements, *J. Geophys. Res.*, *113*, D08204, doi:10.1029/2007JD009388.

Augustine, J. A., C. R. Cornwall, G. B. Hodges, C. N. Long, C. I. Medina, and J. J. DeLuisi (2003), An automated method of MFRSR calibration for aerosol optical depth analysis with application to an Asian dust outbreak over the United States, *J. Appl. Meteorol.*, *42*(2), 266–278, doi:10.1175/1520-0450(2003)042<0266:AAMOMC>2.0.CO;2.

Charlson, R. J., J. E. Lovelock, M. O. Andreae, and S. G. Warren (1987), Oceanic phytoplankton, atmospheric sulfur, cloud albedo and climate, *Nature*, *326*, 655–661, doi:10.1038/326655a0.

Dubovik, O., and M. D. King (2000), A flexible inversion algorithm for retrieval of aerosol optical properties from Sun and sky radiance measurements, *J. Geophys. Res.*, *105*(D16), 20,673–20,696, doi:10.1029/2000JD900282.

Dubovik, O., B. N. Holben, T. F. Eck, A. Smirnov, Y. J. Kaufman, M. D. King, D. Tanré, and I. Slutsker (2002), Variability of absorption and optical properties of key aerosol types observed 20 in worldwide locations, *J. Atmos. Sci.*, *59*, 590–608, doi:10.1175/1520-0469(2002)059<0590:VOAAOP>2.0.CO;2.

Forgan, B. W. (1988), Sun photometer calibration by the ratio Langley method, in *Baseline Atmospheric Program*, edited by B. W. Forgan and P. J. Fraser, pp. 22–26, Bur. of Meteorol., Melbourne, Vic., Australia.

Ge, J. M., J. Su, T. P. Ackerman, Q. Fu, J. P. Huang, and J. S. Shi (2010), Dust aerosol optical properties retrieval and radiative forcing over northwestern China during the 2008 China-U.S. joint field experiment, *J. Geophys. Res.*, doi:10.1029/2009JD013263, in press.

Hansen, J. E., and L. D. Travis (1974), Light scattering in planetary atmospheres, *Space Sci. Rev.*, *16*, 527–610, doi:10.1007/BF00168069.

Hansen, J., M. Sato, and R. Ruedy (1997), Radiative forcing and climate response, *J. Geophys. Res.*, *102*(D6), 6831–6864, doi:10.1029/96JD03436.

Harrison, L., and J. Michalsky (1994), Objective algorithms for the retrieval of optical depths from ground-based measurements, *Appl. Opt.*, *33*, 5126–5132, doi:10.1364/AO.33.005126.

Harrison, L., J. Michalsky, and J. Berndt (1994), Automated multifilter rotating shadow-band radiometer: An instrument for optical depth and radiation measurements, *Appl. Opt.*, *33*, 5118–5125, doi:10.1364/AO.33.005118.

Holben, B. N., et al. (1998), AERONET: A federated instrument network and data archive for aerosol characterization, *Remote Sens. Environ.*, *66*, 1–16, doi:10.1016/S0034-4257(98)00031-5.

IPCC (2007), *Climate Change 2007: The Physical Science Basis. Contribution of Working Group I to the Fourth Assessment Report of the Intergovernmental Panel on Climate Change*, edited by S. Solomon, D. Qin, and M. Manning, Cambridge Univ. Press, Cambridge, U. K.

Irie, H., Y. Kanaya, H. Akimoto, H. Tanimoto, Z. Wang, J. F. Gleason, and E. J. Bucsela (2008), Validation of OMI tropospheric NO_2 column data using MAX-DOAS measurements deep inside the North China Plain in June 2006: Mount Tai Experiment 2006, *Atmos. Chem. Phys.*, *8*, 6577–6586.

Kassianov, E. I., J. C. Barnard, and T. P. Ackerman (2005), Retrieval of aerosol microphysical properties using surface MultiFilter Rotating Shadowband Radiometer (MFRSR) data: Modeling and observations, *J. Geophys. Res.*, *110*, D09201, doi:10.1029/2004JD005337.

Kassianov, E. I., C. J. Flynn, T. P. Ackerman, and J. C. Barnard (2007), Aerosol single-scattering albedo and asymmetry parameter from MFRSR observations during the ARM Aerosol IOP 2003, *Atmos. Chem. Phys.*, *7*, 3341–3351.

Lee, K. H., Z. Li, M. S. Wong, J. Xin, Y. Wang, W.-M. Hao, and F. Zhao (2007), Aerosol single scattering albedo estimated across China from a combination of ground and satellite measurements, *J. Geophys. Res.*, *112*, D22S15, doi:10.1029/2007JD009077.

Lee, K. H., Z. Li, Y. J. Kim, and A. Kokhanovsky (2009), Aerosol monitoring from satellite observations: A history of three decades, in *Atmospheric and Biological Environmental Monitoring*, edited by Y. J. Kim et al., pp. 13–38, Springer, New York, doi:10.1007/978-1-4020-9674-7 2.

Li, Z., et al. (2007a), Preface to special section on East Asian Studies of Tropospheric Aerosols: An International Regional Experiment (EAST-AIRE), *J. Geophys. Res.*, *112*, D22S00, doi:10.1029/2007JD008853.

Li, Z., et al. (2007b), Aerosol optical properties and their radiative effects in northern China, *J. Geophys. Res.*, *112*, D22S01, doi:10.1029/2006JD007382.

Li, Z., et al. (2008), ARM Mobile Facility deployment in China 2008 (AMF-China) science plan, *DOE/SC-ARM-0802*, U.S. Dept. of Energy, Washington, D. C., April.

Li, Z., X. Zhao, R. Kahn, M. Mishchenko, L. Remer, K. H. Lee, M. Wang, I. Laszlo, T. Nakajima, and H. Marig (2009), Uncertainties in satellite remote sensing of aerosols and impact on monitoring its long-term trend: A review and perspective, *Ann. Geophys.*, *27*, 2755–2770.

Mi, W., Z. Li, X. Xia, B. Holben, R. Levy, F. Zhao, H. Chen, and M. Cribb (2007), Evaluation of the moderate resolution imaging spectroradiometer aerosol products at two aerosol robotic network stations in China, *J. Geophys. Res.*, *112*, D22S08, doi:10.1029/2007JD008474.

Michalsky, J. J., J. A. Schlemmer, W. E. Berkheiser, J. L. Berndt, L. C. Harrison, N. S. Laulainen, N. R. Larson, and J. C. Barnard (2001), Multiyear measurements of aerosol optical depth in the atmospheric radiation measurement and quantitative links programs, *J. Geophys. Res.*, *106*, 12,099–12,107, doi:10.1029/2001JD900096.

Nicolet, M. (1981), The solar spectral irradiance and its action in the atmospheric photo dissociation processes, *Planet. Space Sci.*, *29*, 951–974, doi:10.1016/0032-0633(81)90056-8.

Petters, J. L., V. K. Saxena, J. R. Slusser, B. N. Wenny, and S. Madronich (2003), Aerosol single scattering alb6edo retrieved from measurements of surface UV irradiance and a radiative transfer model, *J. Geophys. Res.*, *108*(D9), 4288, doi:10.1029/2002JD002360.

Reagan, J. A., L. W. Thomason, B. M. Herman, and J. M. Palmer (1986), Assessment of atmospheric limitations on the determination of the solar spectral constant from ground based spectroradiometer measurements, *IEEE Trans. Geosci. Remote Sens.*, *GE-24*(2), 258–266, doi:10.1109/TGRS.1986.289645.

Schmid, B., P. R. Spyak, S. F. Biggar, C. Wehrli, J. Sekler, T. Ingold, C. Matzler, and N. Kampfer (1998), Evaluation of the applicability of solar and lamp radiometric calibrations of a precision Sun photometer operating between 300 and 1025 nm, *Appl. Opt.*, *37*, 3923–3941, doi:10.1364/AO.37.003923.

Schotland, R. M., and T. K. Lea (1986), Bias in a solar constant determination by the Langley method due to a structured atmospheric aerosol, *Appl. Opt.*, *25*, 2486–2491.

Shaw, G. E. (1976), Error analysis of multi-wavelength Sun photometry, *Pure Appl. Geophys.*, *114*, 1–14, doi:10.1007/BF00875487.

Shaw, G. E., J. A. Reagan, and B. M. Herman (1973), Investigations of atmospheric extinction using direct solar radiation measurements made with a multiple wavelength radiometer, *J. Appl. Meteorol.*, *12*, 374–380, doi:10.1175/1520-0450(1973)012<0374:IOAEUD>2.0.CO;2.

Tanaka, M., T. Nakajima, and M. Shiobara (1986), Calibration of a Sun photometer by simultaneous measurements of direct-solar and circumsolar radiations, *Appl. Opt.*, *25*, 1170–1176, doi:10.1364/AO.25.001170.

Twomey, S. (1977), The influence of pollution on the short wave albedo of clouds, *J. Atmos. Sci.*, *34*, 1149–1152, doi:10.1175/1520-0469(1977)034<1149:TIOPOT>2.0.CO;2.

Vandaele, A. C., C. Hermans, S. Fally, M. Carleer, R. Colin, M.-F. Merienne, A. Jenouvrier, and B. Coquart (2002), High-resolution Fourier transform measurement of the NO2 visible and near-infrared absorption cross sections: Temperature and pressure effects, *J. Geophys. Res.*, *107*(D18), 4348, doi:10.1029/2001JD000971.

Xia, X., H. Chen, Z. Li, P. Wang, and J. Wang (2007), Significant reduction of surface solar irradiance induced by aerosols in a suburban region in northeastern China, *J. Geophys. Res.*, *112*, D22S02, doi:10.1029/2006JD007562.

H. Chen and X. Xia, LAGEO, Institute of Atmospheric Physics, Chinese Academy of Sciences, Beijing 100029, China.

M. C. Cribb and Z. Li, ESSIC, Department of Atmospheric and Oceanic Science, University of Maryland, College Park, MD 20740, USA.

K. H. Lee, Department of Satellite Geoinformatics Engineering, Kyungil University, 33 Buho-ri, Hayang-eup, Gyeongsan-si, Gyeongsangbuk-do, South Korea 712-701.

B. Li, Center for Atmospheric Observation, China Meteorological Administration, 46 Zhongguancun Nandajie, Haidian district, Beijing 100081, China.

J. Liu, L. Wang, and Y. Zheng, College of Environmental Science and Engineering, Nanjing University of Information Science and Technology, 219 Ning Liu Rd., Nanjing 210044, China.